RATE-SCALABLE UWB FOR WPAN WITH HETEROGENEOUS NODES

Liuqing Yang

Dept. of ECE, Univ. of Florida, P.O.Box 116130, Gainesville, FL 32611

ABSTRACT

The desire for untethered communications spurs increasing interests in wireless sensor networks (WSN) and multimedia communications, including wireless personal area networks (WPAN) with variable rates over a short range. Emerging as a promising candidate for these applications, Ultra-Wideband (UWB) is gaining increasing attention. However, existing research on UWB overlooks one critical issue in enabling seamless network communications: the heterogeneity among network nodes. This paper addresses this issue by designing simple transmission and reception schemes between network nodes with different sampling rates. Our novel communication schemes designed for asymmetric transceiver pairs are readily applicable to achieve seamless communications among heterogeneous network nodes with multi-access capability. We also establish a general system model, which facilitates further delineation and optimization of complexity-performance-rate tradeoffs.

1. INTRODUCTION

Recent development in wireless sensor networks and multimedia communications such as WPANs calls for systems capable of communications among a wide variety of network devices with variable rate, complexity and performance requirements. These requirements motivate research on UWB communications that offer wider range of rates along with enhanced flexibility of complexity-performance-rate tradeoffs [6, 9, 10].

Existing UWB techniques rely on symmetric transmitter and receiver structures, which assume the same complexity level at all nodes throughout the network. In single-band (SB-)UWB, this assumption implies high-rate digital-to-analog (DA) and analog-to-digital (AD) converters at all nodes. These high-rate ADC/DAC's are particularly challenging for UWB radios [5]. In a multi-band (MB-) UWB, this assumption means (multiple) local oscillators and frequency synthesizers at all devices, which are very power consuming and prone to carrier frequency and phase offsets. Estimation and compensation of the latter further aggravate complexity and power consumption. Such transceivers enable high information rate and/or performance improvement, and can certainly be considered for network controllers and rate-critical devices which have more power and computational resources. However, their application to complexity-critical devices is greatly constrained because these nodes are typically small and rely on limited battery power.

To support different types of devices that coexist in a network, transceiver designs need to account for, and take advantage of, the heterogeneity among these nodes. In this paper, we design heterogeneous transceivers with scalable rates and variable complexity levels for different types of network nodes. Due to space limit, we only consider SB-UWB systems with different DAC/ADC rates.

Existing SB-UWB transceiver designs rely on Rake reception, which requires the receiver to sample at higher rate than the transmission rate (see e.g., [3, 8]). But since the forward- and reverse-links utilize the same scheme, transceivers need to be symmetric.

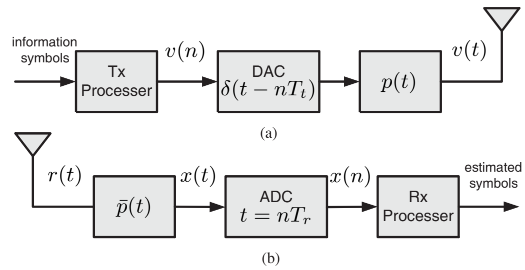

Fig. 1. (a) Transmitter diagram; and (b) Receiver diagram.

The latter, however, is not always the case in a network with different devices. To develop transmission and reception schemes for *asymmetric* transceiver pairs, we establish a general system model that enables delineation of the tradeoffs among complexity, performance and rate. Based on this model, we carefully design transceivers that account for different operating rates at individual nodes and ensure seamless network operation. Our designs are simple: i) they entail a single processing chain at each node; ii) they require minimum modification of transceivers for symmetric links; and iii) the concept of space-time coding can be deployed without employing multiple antennas for multipath diversity collection.

Our general system model is outlined in Section 2. Section 3 derives our novel transceiver designs for asymmetric point-to-point link. In Section 4, these designs are shown to provide rate-scalable multi-access communications among heterogeneous network nodes. Summarizing remarks are given in Section 5.

Notation: $\lceil\cdot\rceil$ and $\lfloor\cdot\rfloor$ stand for integer ceiling and floor operations, respectively; we use boldface uppercase letters for matrices, and lowercase letters for vectors; $\boldsymbol{I}_N$ denotes the $N \times N$ identity matrix, and $\boldsymbol{F}_N$ the $N \times N$ FFT matrix; $\boldsymbol{A}^T$, $\boldsymbol{A}^*$ and $\boldsymbol{A}^{\mathcal{H}}$ stand for transpose, conjugate and Hermitian operations; $\otimes$ denotes Kronecker product.

2. A GENERAL SYSTEM MODEL

The basic transmitter and receiver structures are shown in Fig. 1. The transmitter (Tx) processor may consist of interleaver and/or zero-inserting operators. For multi-carrier (MC-)UWB, the processor also includes (FFT) or discrete cosine transform (DCT) (see e.g. [4, 8]). While the DCT-based MC-UWB does not need an analog carrier, we will use FFT for notational simplicity. The output sequence of the Tx processor $v(n)$ is D/A converted at rate $1/T_t$, pulse shaped by $p(t)$, carrier modulated and transmitted. With the unit-energy pulse shaper $p(t)$ having duration T_p in the order of nanoseconds, the transmission occupies an ultra-wide bandwidth. The transmitted signal per block is then given by:

$$v(t) = \sum_{n=-\infty}^{\infty} v(n)p(t-nT_t)e^{\jmath 2\pi f_c t}, \tag{1}$$

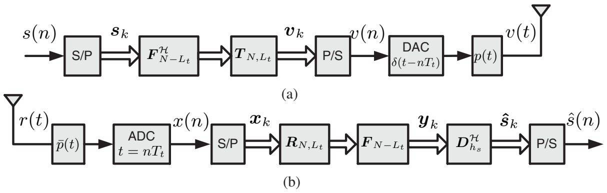

Fig. 2. (a) Transmitter and (b) receiver for a symmetric transceiver pair with $N_r = N_t$.

where f_c is the carrier frequency.[1] Since Eq. (1) allows $T_t \geq T_p$, we let $T_t = N_t T_p$ with integer $N_t \geq 1$.

Let $\tau_{\max}$ denote the maximum multipath delay spread, then the number of resolvable paths is $(L+1)$ with $L := \lfloor \tau_{\max}/T_p \rfloor$. Denoting path gains as $\{h(l)\}_{l=0}^{L}$, the received signal is $r(t) = \sum_{l=0}^{L} h(l) v(t - lT_p)$. It is then frequency demodulated and matched-filtered with $\bar{p}(t) = p(-t)$ to yield

$$x(t) = \sum_{l=0}^{L} h(l) \sum_{n} v(n) R_p(t - nT_t - lT_p) + \eta(t),$$

where $R_p(\tau) := \int p(t)p(t+\tau)dt$ and $\eta(t)$ is the filtered additive Gaussian noise (AGN). Finally, the continuous-time signal $x(t)$ then sampled at interval $T_r := N_r T_p$ with integer $N_r \geq 1$ to obtain the discrete-time sequence $x(m) = \sum_{l=0}^{L} h(l) \sum_n v(n) R_p(mT_r - nT_t - lT_p) + \eta(m)$. It is worth stressing that the receiver ADC rate $1/T_r$ can be different from the transmitter DAC rate $1/T_t$. With $p(t)$ being any Nyquist pulse, we have $R_p(nT_p) = \delta_n$, and

$$x(m) = \sum_{n} v(n) h(mN_r - nN_t) + \eta(m). \qquad (2)$$

Not surprisingly, this discrete-time system model resembles that of a multirate system, because it captures the different sampling rates at the transmitter and the receiver [2]. Through N_t and N_r, this model allows for flexible Tx/Rx processing, including multi-access schemes, as detailed in the ensuing sections.

3. POINT-TO-POINT LINK

In a network with heterogeneous nodes, wireless links should enable communications between: i) symmetric transceivers consisting of same-type nodes; and ii) asymmetric transceivers consisting of different-type nodes. Next, we will discuss three cases: symmetric transceivers with $N_r = N_t$, asymmetric transceivers with $N_r < N_t$ and asymmetric transceivers with $N_r > N_t$.

3.1. Symmetric Transceivers with $N_r = N_t$

In this case, we have

$$x(m) = \sum_{n} v(n) h((m-n)N_t) + \eta(m). \qquad (3)$$

Partitioning sequences $x(m)$, $v(n)$ and $\eta(m)$ into blocks of size N, Eq. (3) can be re-written in a matrix-vector form:

$$\boldsymbol{x}_k = \boldsymbol{H}_s \boldsymbol{v}_k + \breve{\boldsymbol{H}}_s \boldsymbol{v}_{k-1} + \boldsymbol{\eta}_k,$$

provided that $N \geq L_t$ with $L_t := \lfloor \tau_{\max}/T_t \rfloor = \lfloor L/N_t \rfloor$. The $N \times N$ channel matrix $\boldsymbol{H}_s$ is lower-triangular Toeplitz with first column $[h(0), h(N_t), \ldots, h(L_t N_t), 0, \ldots, 0]^T$, and $\breve{\boldsymbol{H}}_s$ is upper-triangular Toeplitz with first row $[0, \ldots, 0, h(L_t N_t), \ldots, h(N_t)]$.

To remove the inter-block interference (IBI) induced by $\breve{\boldsymbol{H}}_s$, zero-padding (ZP) or cyclic-prefix (CP) can be performed at the Tx processor [7]. We will use ZP throughout this paper and represent this operation with the ZP matrix $\boldsymbol{T}_{N,L} := [\boldsymbol{I}_{N-L} \quad \boldsymbol{0}_{N-L,L}]^T$. With the Tx processor being $\boldsymbol{\Theta}_s = \boldsymbol{T}_{N,L_t} \boldsymbol{F}^{\mathcal{H}}_{N-L_t}$, the IBI is removed and we have

$$\boldsymbol{x} = \boldsymbol{H}_s \boldsymbol{T}_{N,L_t} \boldsymbol{F}^{\mathcal{H}}_{N-L_t} \boldsymbol{s} + \boldsymbol{\eta},$$

where the block index k is dropped for notational brevity. Accordingly, the Rx processor also has two parts: $\boldsymbol{\Phi}_s = \boldsymbol{F}_{N-L_t} \boldsymbol{R}_{N,L_t}$, where $\boldsymbol{R}_{N,L_t} := [\boldsymbol{I}_{N-L_t} \quad \boldsymbol{T}_{N-L_t,L_t}]$ renders the channel matrix into a circulant one, and $\boldsymbol{F}_{N-L_t}$ diagonalizes it. Hence, the output at the Rx processor is:

$$\boldsymbol{y} = \boldsymbol{\Phi}_s \boldsymbol{x} = \boldsymbol{F}_{N-L_t} \tilde{\boldsymbol{H}}_s \boldsymbol{F}^{\mathcal{H}}_{N-L_t} \boldsymbol{s} + \tilde{\boldsymbol{\eta}}_s = \boldsymbol{D}_{h_s} \boldsymbol{s} + \tilde{\boldsymbol{\eta}}_s, \qquad (4)$$

where $\tilde{\boldsymbol{\eta}}_s := \boldsymbol{\Gamma}_s \boldsymbol{\eta}$, $\tilde{\boldsymbol{H}}_s := \boldsymbol{R}_{N,L_t} \boldsymbol{H}_s \boldsymbol{T}_{N,L_t}$ and $\boldsymbol{D}_{h_s} := \boldsymbol{F}_{N-L_t} \tilde{\boldsymbol{H}}_s \boldsymbol{F}^{\mathcal{H}}_{N-L_t}$. A symbol detector can be formed as $\hat{\boldsymbol{s}} = (\boldsymbol{D}^{\mathcal{H}}_{h_s} \boldsymbol{D}_{h_s})^{-1} \boldsymbol{D}^{\mathcal{H}}_{h_s} \boldsymbol{y}$. Structure of the symmetric transceiver pair is shown in Fig. 2. From (4), it is clear that OFDM-UWB with $N_t = N_r$ entails a diversity order of 1.

3.2. Asymmetric Transceivers with $N_r < N_t$

In this case, the receiver is a 'heavy' node that operates at a higher rate $1/T_r$ than $1/T_t$ of the relatively 'light' transmitter node. Without loss of generality, let $N_r = N_t/M$ with integer $M > 1$. Eq. (2) then becomes:

$$x(m) = \sum_{n} v(n) h((m - nM)N_r) + \boldsymbol{\eta}(m), \qquad (5)$$

which can be alternatively written as:

$$x(jM+m) = \sum_{n} v(n) h((j-n)N_t + mN_r) + \eta(jM+m), \qquad (6)$$

where $m \in [0, M-1]$. Bearing a form similar to Eq. (3), Eq. (6) can also be cast into a matrix-vector form:

$$\bar{\boldsymbol{x}}_{k,m} = \boldsymbol{H}_m \boldsymbol{v}_k + \breve{\boldsymbol{H}}_m \boldsymbol{v}_{k-1} + \eta_{k,m}, \ \ \forall m \in [0, M-1],$$

where $\bar{\boldsymbol{x}}_{k,m} := [x(kMN+m), x(kNM+m+M), \ldots, x(kNM+m+(N-1)M)]^T$, provided that $N \geq L_{t,m} := \lfloor (L - mN_r)/N_t \rfloor$. The channel matrices $\boldsymbol{H}_m$ and $\breve{\boldsymbol{H}}_m$ are $N \times N$ lower- and upper-triangular Toeplitz with first column $[h(mN_r), h(mN_r + N_t), \ldots, h(mN_r + L_{t,m}N_t), 0, \ldots, 0]^T$ and first row $[0, \ldots, 0, h(mN_r + L_{t,m}N_t), \ldots, h(mN_r + N_t)]$, respectively.

Clearly, to remove IBI $\forall m \in [0, M-1]$, the number of padding zeros in $\boldsymbol{v}_k$ must be no less than $\max_m\{L_{t,m}\}$, which turns out to be L_t. Hence, the Tx processor $\boldsymbol{\Theta}_{a1} = \boldsymbol{\Theta}_s$ can be employed.

By construction, $\bar{\boldsymbol{x}}_{k,m}$ can be obtained by interleaving the sequence $x(n)$. Hence, the first operator at the Rx processor is an interleaver. Further process $\bar{\boldsymbol{x}}_{k,m}$ with $\boldsymbol{\Phi}_{a1} = \boldsymbol{\Phi}_s$, we have:

$$\boldsymbol{y}_m = \boldsymbol{\Phi}_{a1} \bar{\boldsymbol{x}}_m = \boldsymbol{F}_{N-L_t} \tilde{\boldsymbol{H}}_m \boldsymbol{F}^{\mathcal{H}}_{N-L_t} \boldsymbol{s} + \tilde{\boldsymbol{\eta}}_m = \boldsymbol{D}_{h_m} \boldsymbol{s} + \tilde{\boldsymbol{\eta}}_m, \qquad (7)$$

where the block index k is dropped, and $\tilde{\boldsymbol{H}}_m$, $\boldsymbol{D}_{h_m}$ and $\tilde{\boldsymbol{\eta}}_m$ are defined similar to $\tilde{\boldsymbol{H}}_s$, $\boldsymbol{D}_{h_s}$ and $\tilde{\boldsymbol{\eta}}_s$, respectively.

Notice that with a single input vector $\boldsymbol{s}$, we have collected multiple copies $\{\boldsymbol{y}_m\}_{m=0}^{M-1}$ at the receiver, as a result of over-sampling with factor M. Symbol estimates can then be formed via maximum ratio combining (MRC) as:

$$\hat{\boldsymbol{s}} = \sum_{m=0}^{M-1} (\boldsymbol{D}^{\mathcal{H}}_{h_m} \boldsymbol{D}_{h_m})^{-1} \boldsymbol{D}^{\mathcal{H}}_{h_m} \boldsymbol{y}_m.$$

Different from Eq. (4), a diversity order of M is observed here. Similar observations are also made in the context of Rake reception (see e.g., [3, 8]). As depicted in Fig. 3, the transmission scheme corresponding to $N_r < N_t$ is the same as that of $N_r = N_t$, which means no modification is needed at the 'light' node. At the receiver side, an interleaver is added when $N_r < N_t$, as shown in Fig. 2(b).

[1]If $v(n)$ is real and $p(t)$ is compliant with the FCC spectral mask, then carrier modulation with f_c is not needed.

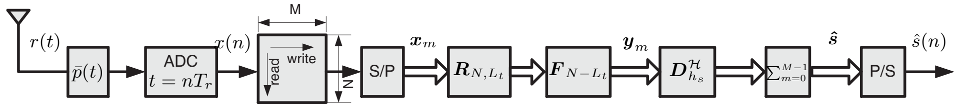

Fig. 3. Receiver for an asymmetric transceiver pair with $N_r = N_t/M$.

3.3. Asymmetric Transceivers with $N_r > N_t$

Now the transmitter is a 'heavy' node that operates at a higher rate $1/T_t$ than $1/T_r$ of the relatively 'light' receiver node. Let $N_r = MN_t$ with integer $M > 1$ being a factor of N. Eq. (2) becomes $x(m) = \sum_n v(n)h((mM - n)N_t) + \eta(m)$, or equivalently:

$$x(m) = \sum_j \sum_{n=0}^{M-1} v(jM + n)h((m - j)N_r - nN_t) + \eta(m).$$

Similar to (3) and (6), its corresponding matrix-vector form is:

$$\boldsymbol{x}_k = \sum_{n=0}^{M-1} \left(\boldsymbol{H}_n \bar{\boldsymbol{v}}_{k,n} + \breve{\boldsymbol{H}}_n \bar{\boldsymbol{v}}_{k-1,n} \right) + \boldsymbol{\eta}_k,$$

where $\boldsymbol{x}_k := [x(kN), x(kN + 1), \ldots, x(kN + N/M - 1)]^T$ and $\boldsymbol{v}_{k,n} := [v(kN+n), v(kN+n+M), \ldots, v(kN+n+N-M)]^T$ are both $N/M \times 1$ vectors, the N/M by N/M channel matrices $\boldsymbol{H}_n$ and $\breve{\boldsymbol{H}}_n$ are lower- and upper-triangular Toeplitz matrices with first column $[h(-nN_t), h(N_r - nN_t), \ldots, h(L_{r,k}N_r - nN_t), 0, \ldots, 0]^T$ and $[0, \ldots, 0, h(L_{r,k}N_r - nN_t), \ldots, h(N_r - nN_t)]^T$, respectively, with $L_{r,n} := \lfloor (L + nN_t)/N_r \rfloor$.

To remove IBI $\forall n \in [0, M - 1]$, we need $\boldsymbol{v}_{k,n}$ to have at least $L_{r,n}$ trailing zeros. In order to use the same ZP matrix $\forall n$, vectors $\{\boldsymbol{v}_{k,n}\}_{n=0}^{M-1}$ should all have $\max_n\{L_{r,n}\} = L_r := \lceil L_t/M \rceil$ trailing zeros. The latter translates to ML_r trailing zeros at each transmitted symbol vector $\boldsymbol{v}_k$.

With $\boldsymbol{\Theta}_{a2} := \boldsymbol{T}_{N,ML_r}\boldsymbol{F}_{N-ML_r}^{\mathcal{H}}$ at the high-rate transmitter and $\boldsymbol{\Phi}_{a2} := \boldsymbol{F}_{N/M-L_r}\boldsymbol{R}_{N/M,L_r}$ at the low-rate receiver, we have proved that:

$$\boldsymbol{y} = \boldsymbol{\Phi}_{a2}\boldsymbol{x} = \sum_{m=0}^{M-1} \boldsymbol{\mathcal{D}}_{h_m}\boldsymbol{s}_m + \tilde{\boldsymbol{\eta}}, \tag{8}$$

where $\tilde{\boldsymbol{\eta}}$ is the filtered AWGN,

$$\boldsymbol{\mathcal{D}}_{h_m} := \sum_{n=0}^{M-1} \boldsymbol{D}_{h_n} \operatorname{diag}\left\{1, e^{\jmath\frac{2\pi m}{N-ML_r}}, \ldots, e^{\jmath\frac{2\pi m(N/M-L_r-1)}{N-ML_r}}\right\} e^{\jmath\frac{2\pi mn}{M}}$$

and $\boldsymbol{D}_{h_n}$ is the diagonalized channel defined similar to $\boldsymbol{D}_{h_s}$ in (4).

To enable symbol detection and diversity collection, one could perform MRC at the transmitter (a.k.a. pre-Rake) by letting $\boldsymbol{s}_m = (\boldsymbol{\mathcal{D}}_{h_m}^{\mathcal{H}}\boldsymbol{\mathcal{D}}_{h_m})^{-1}\boldsymbol{\mathcal{D}}_{h_m}^{\mathcal{H}}\boldsymbol{s}$. But this approach entails channel state information (CSI) at the transmitter. Alternatively, noticing that Eq. (8) is simply a multi-input single-output (MISO) system, we can apply space-time coding (STC) techniques developed for multiple transmit- and a single-receive antennas. Take $M = 2$ as an example. In this case, we can transmit $\boldsymbol{s}_0 = \boldsymbol{s}_a$ and $\boldsymbol{s}_1 = \boldsymbol{s}_b$ during the first period of NT_t, and $\boldsymbol{s}_0 = -\boldsymbol{s}_b^*$ and $\boldsymbol{s}_1 = \boldsymbol{s}_a^*$ during the following period of NT_t. The two consecutive Rx processor outputs are:

$$\bar{\boldsymbol{y}} := \begin{bmatrix} \boldsymbol{y}_0 \\ \boldsymbol{y}_1^* \end{bmatrix} = \begin{bmatrix} \boldsymbol{\mathcal{D}}_{h_0} & \boldsymbol{\mathcal{D}}_{h_1} \\ \boldsymbol{\mathcal{D}}_{h_1}^* & -\boldsymbol{\mathcal{D}}_{h_0}^* \end{bmatrix} \begin{bmatrix} \boldsymbol{s}_a \\ \boldsymbol{s}_b \end{bmatrix} + \begin{bmatrix} \tilde{\boldsymbol{\eta}}_0 \\ \tilde{\boldsymbol{\eta}}_1^* \end{bmatrix} := \boldsymbol{\mathcal{D}}_h\bar{\boldsymbol{s}} + \begin{bmatrix} \tilde{\boldsymbol{\eta}}_0 \\ \tilde{\boldsymbol{\eta}}_1^* \end{bmatrix},$$

which leads to a symbol estimator: $\hat{\bar{s}} = (\boldsymbol{\mathcal{D}}_h^{\mathcal{H}}\boldsymbol{\mathcal{D}}_h)^{-1}\boldsymbol{\mathcal{D}}_h^{\mathcal{H}}\bar{\boldsymbol{y}}$. It is worth emphasizing that although this scheme is similar to STC with two transmit- and one-receive antennas in [1], the coding here is performed only in time-domain and only a single antenna is employed at the transmitter. But similar to STC, such a coding scheme enables multipath diversity order of M. Therefore, we term it diversity encoding and decoding. Transceiver structures with $N_r > N_t$ are shown in Fig. 4. Comparing them with the symmetric structures in Fig. 2, we notice that the only differences are the diversity codecs.

So far, we have shown that one-to-one communication between heterogeneous nodes not only is possible, but also facilitates flexible complexity-performance tradeoff and rate scalability. Equally important is that such schemes can be implemented with minimum modification of existing systems.

In a network, one node often needs to communicate with multiple nodes simultaneously, while these target nodes may operate at different rates. We will investigate this issue in the ensuing section.

4. MULTI-ACCESS LINK

Let us consider a network with two types of nodes: one type operates at rate $1/T_L$ and the other at $1/T_H$, for both transmission and reception. Let $T_L = MT_H$ with integer $M > 1$ and term them L ('low' or 'light') and H ('high' or 'heavy') nodes, respectively. Clearly, H-nodes requires higher ADC/DAC rate. In WPANs, the piconet controllers and rate-critical devices can be H-nodes, whereas complexity-critical devices can be L-nodes. Next, we will show that: i) an H-node can communicate with H and L nodes simultaneously, while the H-H information rate can be higher than the H-L rate; and ii) an L-node can communicate with H and L nodes at the same rate, but with different diversity gains.

4.1. L-Node Centered Multi-Access

Without loss of generality, suppose that only two nodes are communicating with the center L-node: one is L-node and the other is H-node. As detailed in Section 2, the symmetric L-L link and the asymmetric L-H link share the same transmitter structure with rate $1/T_L$. Thus, the transmitter in Fig. 1(a) can be directly adopted.

In MC-UWB, multi-access can be achieved by assigning distinct carriers to different users. To do this, we define the $(N - L_t) \times C_L$ carrier selection matrix (CSM) $\boldsymbol{S}_L$ that assigns C_L distinct carriers to the L-node. It can be shown that columns of $\boldsymbol{S}_L$ are distinct columns of the $\boldsymbol{I}_{N-L_t}$. Similarly, we define the $(N - L_t) \times C_H$ CSM $\boldsymbol{S}_H$ for the H-node. The transmitted block $\boldsymbol{v}$ is then given by [c.f. Section 3.1]:

$$\boldsymbol{v} = \boldsymbol{\Theta}_s(\boldsymbol{S}_L\boldsymbol{s}_L + \boldsymbol{S}_H\boldsymbol{s}_H).$$

If $\boldsymbol{S}_H$ and $\boldsymbol{S}_L$ are orthogonal, i.e., $\boldsymbol{S}_L^T\boldsymbol{S}_H = \boldsymbol{0}_{C_L \times C_H}$, then there is no interference. The noise-free Rx processor output at the L-node is [c.f. (4)]:

$$\boldsymbol{y}_L = (\boldsymbol{S}_L^T\boldsymbol{D}_{h_s}\boldsymbol{S}_L)\boldsymbol{s}_L.$$

Using Eq. (7), the noise-free Rx processor output at the H-node can also be obtained:

$$\boldsymbol{y}_{H,m} = (\boldsymbol{S}_H^T\boldsymbol{D}_{h_m}\boldsymbol{S}_H)\boldsymbol{s}_H, \ \ \forall m \in [0, M - 1].$$

Symbol detection is then straightforward. Since the H-node receives M copies of the transmitted symbol block, it is capable of collecting the diversity order of M. The L-node, on the other hand, only receives a single copy but with lower complexity. Their different diversity orders determine their bit-error-rate (BER) performance,

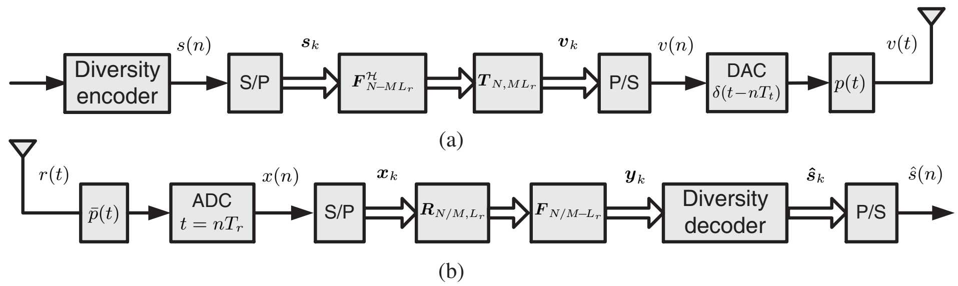

Fig. 4. Receiver for an asymmetric transceiver pair with $N_r = MN_t$.

as shown in Fig. 5. Further notice that when $C_L = C_H$, the L-L link and the L-H link have the same rate. This is because the center L-node is the rate-limiting side. As we will see next, selecting an L-node as a center node does not provide as much flexibility and rate scalability as selecting an H-node as a center node.

4.2. H-Node Centered Multi-Access

As detailed in Section 3, the only difference between the symmetric H-H link transmitter and the asymmetric H-L link transmitter is the diversity encoder. Hence, we can use the same transmitter structure while encoding the data to L-node before feeding it to the Tx processor.

To enable multi-access, CSM's can be used. But in this case, special considerations are needed. We proved that the CSM's for the target L- and H-nodes are $\boldsymbol{I}_M \otimes \boldsymbol{S}_L$ and $\boldsymbol{I}_M \otimes \boldsymbol{S}_H$, where $\boldsymbol{S}_L$ and $\boldsymbol{S}_H$ are $(N/M - L_r) \times C_L$ and $(N/M - L_r) \times C_H$ CSM's satisfying $\boldsymbol{S}_L^T \boldsymbol{S}_H = \boldsymbol{0}_{C_L \times C_H}$. Intuitively, this is because smaller FFT matrices are employed at the L-nodes.

It can be shown that the noise-free Rx processor output at the L-node receiver are $C_L \times 1$ vectors [c.f. (8)]

$$\boldsymbol{y}_L = \sum_{m=0}^{M-1} (\boldsymbol{S}_L^T \boldsymbol{\mathcal{D}}_{h_m} \boldsymbol{S}_L) \boldsymbol{s}_{L,m},$$

where $\boldsymbol{s}_{L,m}$ are $C_L \times 1$ information sub-vectors for the L-node. Using 4, the $MC_H \times 1$ noise-free output at the H-node can be easily obtained:

$$\boldsymbol{y}_H = (\boldsymbol{I}_M \otimes \boldsymbol{S}_H^T) \boldsymbol{D}_{h_s} (\boldsymbol{I}_M \otimes \boldsymbol{S}_H) \boldsymbol{s}_H.$$

As aforementioned, symbol sub-blocks $\{\boldsymbol{s}_{L,n}\}_{n=0}^{M-1}$ for the L-node are repeated either across sub-blocks (with the pre-Rake option) or across blocks (with the diversity coding option). But $\boldsymbol{s}_H$ for the H-node can contain up to MC_H distinct symbols. Therefore, even with $C_L = C_H$, the maximum rate for the H-H link is M times that of the H-L link. By introducing redundancy, the H-L link enables a diversity order of M; whereas the H-H link provides a wider range of performance-rate tradeoff at the price of higher sampling rate.

5. CONCLUSIONS

We developed asymmetric UWB links for wireless networks with heterogeneous nodes. These links facilitate multi-access communications, without sacrificing rate-scalability and complexity at individual nodes. Exploiting the high sampling rate at 'heavy' nodes while maintaining the low-complexity at 'light' nodes, our seamless schemes turn out to be simple. They entail a single processing chain with minimum modification on transceivers for symmetric links, and can take advantage of the well-developed STC techniques. Such designs allow network nodes to have variable complexity and power consumption, and can prolong the lifetime of the entire network, especially the power-critical devices.

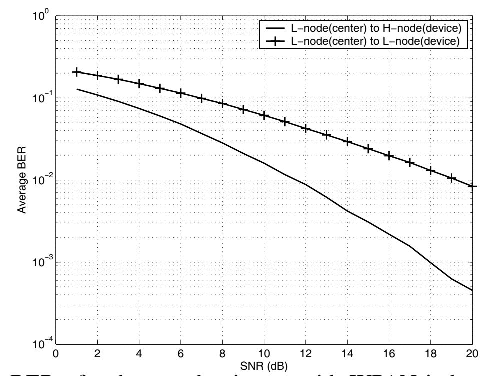

Fig. 5. BER of a three-node piconet with WPAN indoor channel model. Data rate is 200Mbps for each device node. Transmission bandwidth is 1GHz. $T_L = 2T_H$.

6. REFERENCES

[1] S. M. Alamouti, "A simple transmit diversity technique for wireless communications," *IEEE JSAC*, vol. 16, no. 8, pp. 1451–1458, October 1998.

[2] R. E. Crochiere and L. R. Rabiner, *Multirate Digital Signal Processing*. Prentice Hall, 1996.

[3] G. Durisi, A. Tarable, J. Romme, and S. Benedetto, "A general method for error probability computation of UWB systems for indoor multiuser communications," *J. of Comm. and Networks*, vol. 5, no. 4, pp. 354–364, December 2003.

[4] D. Gerakoulis and P. Salmi, "An interference suppressing ofdm system for ultra wide bandwidth radio channels," in *Proc. of UWBST*, Baltimore, MD, May 20-23, 2002, pp. 259–264.

[5] S. Hoyos, B. Sadler, and G. Arce, "High-speed A/D conversion for ultra-wideband signals based on signal projection over basis functions," in *Proc. of ICASSP*, vol. 4, Montreal, Quebec, Canada, May 17-21, 2004, pp. 537–540.

[6] S. Roy, J. Foerster, V. Somayazulu, and D. G. Leeper, "Ultra-wideband radio design: the promise of high-speed, short-range wireless connectivity," *Proc. of the IEEE*, vol. 92, no. 2, pp. 295–311, February 2004.

[7] Z. Wang and G. B. Giannakis, "Wireless multicarrier communications: Where Fourier meets Shannon," *IEEE Signal Processing Mag.*, vol. 17, no. 3, pp. 29–48, May 2000.

[8] L. Yang and G. B. Giannakis, "Digital-carrier multi-band user codes for baseband UWB multiple access," *Journal of Comm. and Networks*, vol. 5, no. 4, pp. 374–385, December 2003.

[9] ——, "Ultra-wideband communications: An idea whose time has come," *IEEE Signal Processing Mag.*, vol. 21, no. 6, pp. 26–54, November 2004.

[10] W. Zhuang, X. Shen, and Q. Bi, "Ultra-Wideband wireless communications,," *WCMC*, vol. 3, no. 6, pp. 663–685, 2003.